International Journal of Adhesion & Adhesives 102 (2020) 102641

Contents lists available at ScienceDirect

International Journal of Adhesion and Adhesives

journal homepage: http://www.elsevier.com/locate/ijadhadh

Coating adhesion of a chromate-containing epoxy primer on Al2024-T3 surface processed by laser-interference

Adrian S. Sabau [a,*], Jiheon Jun [b], Dana McClurg [b]

[a] Computational Sciences & Engineering Division, Oak Ridge National Laboratory, 1 Bethel Valley Road, Oak Ridge, TN, 37831, USA
[b] Materials Science and Technology Division, Oak Ridge National Laboratory, 1 Bethel Valley Road, Oak Ridge, TN, 37831, USA

ARTICLE INFO

Keywords:
Primers and coupling agents (A)
Aluminium and alloys (B)
Adhesion by mechanical interlocking (D)
Laser

ABSTRACT

In this study, the coating adhesion test results are presented for a primer that was coated on laser-interference structured surfaces of as-received Al2024-T3 specimens, i.e., without employing any polishing, cleaning, or any other surface alteration techniques. All of the laser-interference processing was performed by splitting the primary beam of a Q-switched Nd:YAG pulsed nanosecond laser into two beams and focused them to the same spot. The specimens were spray painted with a chromate-containing epoxy primer, CA7233, compliant to MIL-PRF-23377 Type I Class C2 specification. The adhesion of primer on Al surface with different treatments was assessed using the ASTM D3359 X-cut and cross-hatch tests. It was found that the laser processed specimens meet the performance requirements in the coating adhesion specifications by having a higher or identical ranking for coating adhesion specimens than those prepared with current state-of-the-art chemical conversion or sulfuric acid anodizing. The rastering with either 4 mm/s or 6 mm/s with a laser fluence of 1.78 J/cm^2 is recommended to attain acceptable coating adhesion, even higher than that with the anodizing surface treatment.

These results indicate that laser-interference shows significant potential as a non-chemical surface preparation technique for these coatings.

1. Introduction

In this study, data on coating adhesion for laser-interference surface treatments of aluminum alloy AA 2024-T3 is presented with the aim of identifying laser processing parameters that would be considered acceptable to pass the adhesion requirements. Passing the coating adhesion tests is prerequisite for more comprehensive corrosion testing. The aluminum alloy AA 2024-T3 is used extensively in aerospace applications due to its excellent strength-to-weight ratio and relatively low cost (Brown [1]). Due to its susceptibility to localized corrosion, which was found to affect its service performance, Al2024 surfaces need to be protected. For protective coating application, the surface of Al alloys is commonly pre-treated to enhance both the adhesion between the substrate and primer for corrosion resistance. Conversion coatings with corrosion inhibitors and anodizing treatments have been used widely for the pre-treatment of Al surface. For conversion coatings, hexa-chromates are the most common inhibitors. As shown in Fukuda Fukushima [2], anodizing treatments are conducted in highly acidic solutions under high anodic potentials to form an alumina-based surface layer with its unique columnar pores. After anodizing, a sealing treatment can be used to fill the pores of the anodized layer with hot water where some inhibitors can also be added to improve corrosion resistance (e.g., González et al. [3]). Conversion coating and anodizing treatments, however, require the use of harmful chemicals and produce the chemical wastes, increasing the process and disposal costs for these surface treatments. Thus, other alternative inhibitors, such as tri-chromate and non-chromate inhibitors, which were used by Pearlstein and Agarwala [4] and Campestrini et al. [5], respectively, were also studied to reduce the use of toxicity intrinsic to the hexa-chromates.

Another way to minimize the use of toxic inhibitors is through novel non-chemical surface treatments. Laser-based surface treatments, that can be used for coating removal and surface cleaning for Al alloys (such as in Critchlow et al. [6]), were shown to strengthen bonding between Al surface and adhesive. The improved adhesion by laser treatment was previously attributed by Critchlow et al. [6] to the removal of organic contaminants, and by Langer et al. [7] to the increased surface roughness which promotes interlocking between the adhesive and Al alloys. Critchlow et al. [6] and Langer et al. [7] and all of the studies on this topic used a single-beam laser setup. Kai et al. [8] found that short-pulse lasers, such as excimer lasers, were found to provide a mechanism for

* Corresponding author.
E-mail address: sabaua@ornl.gov (A.S. Sabau).

https://doi.org/10.1016/j.ijadhadh.2020.102641
Received 27 March 2020; Accepted 24 April 2020
Available online 19 May 2020
0143-7496/© 2020 Elsevier Ltd. All rights reserved.

changing the surface morphology without significant damage to the underlying material. However, these proof-of-principle studies were conducted using laser systems that employed small laser beam sizes, e.g., between 10 and 500 μm, without large scale application of the structuring.

Unlike in all previous studies aimed at laser treatment surfaces of Al2020-T3, specimens were treated in this study using a Q-switched Nd:YAG based on a laser-interference technique, as shown by Daniel et al. [9] and Lasagni et al. [10]. The laser interference power profile was created by splitting the beam and guiding those beams to the sample surface by overlapping each other with defined angles. The coherent beams was shown to create an interference pattern, such as dot-, line-, and ring-shaped by Daniel et al. [9] and Sabau et al. [11]. Recently, Meyer et al. [12] showed that the solidification under high cooling rates for short-pulse lasers was found to offer the possibility to obtain new phases, surface compositions, and/or surface microstructures. To the best of our knowledge, this study is the first to investigate the use of the laser-interference structuring (LIS) for surface preparation as a non-contact process, i.e., without abrasion or additional chemicals.

Considering the aerospace applications, a commercial primer, Desoprime™ HS CA7233 Military Epoxy Primer (PPG Aerospace Coatings), which complies MIL-PRF-23377 specification [13] was selected in this study. The chromate-based epoxy primer was spray painted on the aluminum surfaces treated with LIS, conversion coatings or anodization, and the adhesion of the primer was estimated. To assess the adhesion of coating systems, Troconis and Frankel [14] used the blister test, pull-off test [15], peel test [16], and scratch tests [16]. Among the listed tests, the scratch-based tests, such as X-cut and cross-hatch, are relatively simple to conduct and provide quantitative assessment of adhesion strength according to the ASTM D 3359 standard [16]. In these scratch tests, X-cut or cross-hatch patterned scribes are made through the coating and then a standard-specified tape is used to delaminate coating on the scribed surface. After the removal of the tape, a semi-quantitative adhesion rating can be assigned by analyzing delimited area along the scribes [16]. These scratch tests have been used by Subasri et al. [17] and Alrashed et al. [18] to assess the adhesion of primer alone or primer with top-coat.

As part of a larger effort to investigate a laser-based surface treatment as a non-chemical surface preparation for aerospace coating systems, the goal of this study is to identify laser-interference processing parameters for which the primer-coated Al2024 surfaces would pass the coating adhesion requirements. The paper is organized as follows. First, materials, surface preparation, and testing methodology are introduced. Second, results for the surface profile and roughness are presented for the as-received and laser structured conditions. Third, the results for the adhesion of the primer coating according to ASTM D3359 using the X-cut and cross-hatch scratch tests are presented. Data on the dependence of coating adhesion on the laser fluence and laser raster speed is presented and discussed. The effect of the coating thickness, and storage time prior to coating application on the coating adhesion is also discussed.

2. Materials and experimental procedures

2.1. Materials

Bare Al 2024-T3 panels with the surface area of 50 mm × 50 mm or 75 mm × 75 mm and the thickness of 0.81 mm (0.032 in) were obtained from an external vendor. All of the Al 2024-T3 with control pretreatments, namely chromated conversion coated (CCC) and sulfuric acid anodized (SAA), were obtained from the Q-LAB vendor (Westlake, OH). According to the vendor's report, CCC treatment was completed using a hexa-chromate agent according to MIL-DTL-5541 type I (with hexavalent Cr), and SAA panels were sealed using hot water without corrosion inhibitors according to MIL-DTL-8625 type II, Class 1. For the laser structuring, the 2024-T3 0.813 mm (0.032 in) gauge sheet material was certified to meet the ASTMB209, AMS-QQA250/4, and AMS4037 standards by the supplier. The thicknesses of CCC and SAA Al 100 mm × 150 mm panels were also 0.813 mm (0.032 in). The CCC and SAA panels were cut to the size of 50 mm × 75 mm using a shear cutter. The thickness of chromated and anodized layers was measured at the center and four spots diagonally 1 cm away from each corner (total five spots) per panel. A commercial thickness gage (DeFelsko) using ultrasonic reflection for the thickness measurement was used. In 15 CCC panels, the average thickness of chromate layer was below the detection limit, i.e. 0.5 μm. In 15 SAA panels, the average thickness of anodized layer was approximately 4 μm.

A commercially available CA7233 primer kit, compliant to MIL-PRF-23377 Type I Class C2 specification, was selected in this work. Desoprime™ HS CA7233 Military Epoxy Primer was prepared by mixing by volume one part of CA 7233A base and one part of CA 7233B activator. Primers for this military specification were manufactured by PPG Industries, Inc. This primer product contained strontium chromate as corrosion inhibitor.

2.2. Laser-interference structuring

A 10Hz Q-switched Nd:YAG laser (Quanta-Ray PRO 230, Spectra Physics) was used in this study. The fundamental emission with the wavelength of 1064 nm was transformed to 355 nm using non-linear crystals. At 355 nm wavelength, the pulse duration was ~8 ns, resulting in an extremely high peak power above 100 MW and greater than 10^{12}K/s heating rates. The laser interference power profile was created by splitting the beam and guiding those beams to the sample surface by overlapping each other with defined angles as indicated by Daniel et al. [9]. The coherent beams create an interference pattern instead of just adding their intensity. This allows a microscopic modulation and creates a light pattern without loss of energy during the interference process. As shown by Lasagni et al. [10] LIS patterns can be dot-, line-, and ring-shaped. The laser pulse fluence (pulse energy per unit area) was increased by using two identical focal lenses in each path of the beams to focus them to 6 mm spot size, a smaller spot from its original size of 8 mm as used by Sabau et al. [11] and Meyer et al. [12]. The periodicity between power peaks and laser-interference induced undulations (d), is defined by the wavelength, λ, and the angle, α, between the two beams, as:

$$d = \frac{\lambda}{2sin(\alpha/2)} \tag{1}$$

The surface morphology has the following characteristics: (a) undulation spacing of 0.5–50 μm, (b) structured area of 0.27cm^2/shot, and (c) scanning speed: 10,000 lines at a time, 79 million dots at a time, up to 162 cm^2/min. The specimens were processed in raster mode in which the sample was translated while the laser was on at all times. At the end of each line scan, the specimen was then positioned normal to the main scanning direction such that the next line scan will be laser processed. The overlap between adjacent rows of scans was 1 mm. The scan direction was identical to that of the rolling direction. The beam angle was 12°, for a theoretical periodicity of the structures of approximately 1.7 μm. In this study, two laser fluences of $F_1 = 1.238$ and 1.782 J/cm^2 per pulse were used by varying the laser spot size ($d_b = 6$ and 5 mm, respectively) while keeping the same average power of 3.5 W. The pulse repetition rate was $f_L = 10$ Hz. In order to quantify the effect rastering speed, U, of the laser beam on the energy deposited on the specimen surface, the two process variables were introduced: (a) the number of equivalent pulses, N_P, and (b) the accumulated fluence on specimen surface, F_A. N_P represents the number of pulses that a local area is exposed while the F_A represent the total incident laser energy that a local area would be exposed from the total N_P pulses striking it as the laser beam is scanned over it. For the sake of simplicity, N_P is defined at the centerline while the fluence of each shot is considered to be simply that for a single laser shot, F_1, as:

$$N_P(U) = \frac{d_b \cdot f_L}{U} \quad and \tag{2}$$

$$F_A = N_P \cdot F_1. \tag{3}$$

The number of equivalent pulses, N_P, and the accumulated fluence on specimen surface, F_A, are given in Table 1. At 2 mm/s raster speed, the surface is exposed to approximately 30 shots with an accumulated fluence of approximately 37 J/cm^2. As the raster speed is increased, the surface is exposed to a smaller number of shots and smaller accumulated fluences.

2.3. Profilometry and roughness analysis procedures

A WYKO NT9100 surface profilometer was used to obtain surface roughness data for the alloy surfaces in the as–received condition, i.e., without any laser processing, and after laser-interference processing. Wyko optical surface profilometer systems, which was supplied by Veeco Instruments Inc., are non-contact optical profilers that can be used to measure a wide range of surface topographical features. The area chosen for surface profiling was located along the centerline of a laser scan. A magnification of 50× was used for surface profiling.

The average roughness, or arithmetical mean deviation of the roughness profile, R_a, root-mean-square deviation of the roughness profile, R_q, maximum roughness, R_z, and maximum height of the roughness profile, Rt, were included in the analysis. R_a was calculated by averaging the absolute height variation within the sampling length by excluding a few outlying points so that the extreme points have no significant impact on the final results. By contrast, profile extremes have a much greater influence on R_z, which is an absolute vertical variation between the maximum profile peak height and the maximum profile valley depth along the sampling length. Usually, R_z averages the five highest peaks and the five deepest valleys. R_t is height variation between the maximum profile peak height and the maximum profile valley depth along the sampling length.

2.4. Primer coating procedure

Both the laser-structured specimens and the controlled specimens were stored either in plastic cases in order to avoid air contaminants and humidity effects for several days, weeks, and even months prior to coating application. Each specimen was laid in its own plastic case with the LIS surface facing up such that the LIS surface did not touch the plastic case surface. The storage duration of the LIS specimens prior to coating application, is often referred in industry as to open-time, t_o. The open-time was recorded for all LIS specimens in order to study any possible degradation of the coating adhesion with the open time.

The procedure for the primer coating operation on Al panels was conducted as follows. For pre-cleaning of control specimens, the Al surface was rinsed with ethanol and gently wiped with a dust-free cloth. The surface of the laser structured specimens was *not* cleaned at all prior to the laser processing. The cleaned control panels and "uncleaned" laser structured panels were loaded on a paint rack and spray-coated with CA7233 primer using a spray gun operated with the nozzle pressure of 0.138 MPa. The painting of primer was conducted within the allowable temperature range (20–30 °C) and below the upper humidity limit of 65%. The coated Al panels were then dried in a fume hood for 24 h to allow evaporation of volatile species and subsequently cured in an oven at 60 °C for 24 h.

Table 1
Energy metrics for several raster speeds for laser fluences F_1 of 1.238 and 1.782 J/cm^2.

F_1 [J/cm^2]	1.238		1.782	
U [mm/s]	N_P	F_A [J/cm^2]	N_P	F_A [J/cm^2]
4	15	18.57	13	22.28
6	10	12.38	8	14.85
8	7	9.28	6	11.14
10	6	7.43	5	8.91

2.5. Coating adhesion test procedures and process variables

Following oven curing, the thickness of the primer on Al panels was measured using the same DeFelsko thickness gage that was used for measuring the anodized thickness layer. For each panel, the primer thickness was measured at the center and 4 spots diagonally 1 cm away from each corner for a total of five measurements per panel. The average Coating Thickness (CT) was obtained from these five measurements. It should be noted that the coating thickness of SAA panels includes both that of the primer and ~4 μm thick anodized layer. Per manufacturer specifications, the recommended thickness of the primer coating is 15–30 μm.

The adhesion performance of primer coating was tested and assessed according to ASTM D3359 which specifies X-cut and cross-hatch scratch test procedures and the criteria of adhesion rating [16]. The adhesion rating of both scratch tests is based on 0–5 scale increasing by 1 with 0 and 5 assigned for the lowest and highest adhesion. The X-cut tape adhesion testing was conducted according to procedures from section seven of ASTM D3359. An X-cut was made through the coating to the substrate using a pencil type scribing tool with carbide stylus, then a pressure-sensitive tape was applied over the cut. Within 60–120 s of tape application, tape was removed by pulling it off rapidly back upon itself at as close to an angle of 180° as possible. The coating adhesion rating was assigned by examining the X-cut coating area, which was removed from the substrate or previous coating, in accordance with the scale classification shown from ASTM D3359 (section 7). The X-cut test is easier to perform than the cross-hatch test.

The cross-hatch adhesion tests were conducted according to ASTM D3359, Section 12. A Paint Adhesion Test (PAT) kit was purchased from Paul N. Gardner Company, Inc., including the PA-2000 handle and the cutter PA-2053 (1.0 mm blade spacing with 11 teeth). The coating adhesion rating for the cross-hatch test was evaluated by examining the grid area for removal of coating from the substrate using a magnifier, and rating the adhesion for according with the scale classification. The X-cut test is considered in industry as a less severe test than the cross-hatch test. Thus, more specimens were tested for the cross-hatch test than for the X-cut test, once the X-cut tests indicated that the laser structured specimens would pass this test.

3. Results for surface morphology

The profiling surface covered an area of 130 × 174 μm. The 3D height distributions of typical surfaces in the as-received, and unprocessed condition and after laser-interference processing are shown in Fig. 1. The surface profiles for the as-received surfaces are shown in Fig. 1a and b for two specimens. The first specimen contains areas that were laser processed with scanning speeds of 2 and 4 mm/s while the second specimen contains areas processed with scanning speeds of 6 and 8 mm/s. The surface profiles are shown in Fig. 1 for all laser scanning speeds of 2, 4, 6, and 8 mm/s in Fig. 1c, d, 1e, and 1f, respectively. The laser scan direction was identical to that of the rolling direction.

Optical images obtained with the profilometer are shown for the sake of completion in Fig. 2 while high-resolution scanning electron microscopy (SEM) images for these laser processing conditions are recently presented in Meyer et al. [19]. Due to the height variation and optical limitations, some regions would appear out of focus in the optical micrographs, however, the information from the profilometry and its corresponding optical image are complimentary. For example, the surface defects intrinsic to the prior rolling operations and interference-induced structuring is more evident in the optical micrographs than in the 2D profilometry images. For better detail, optical

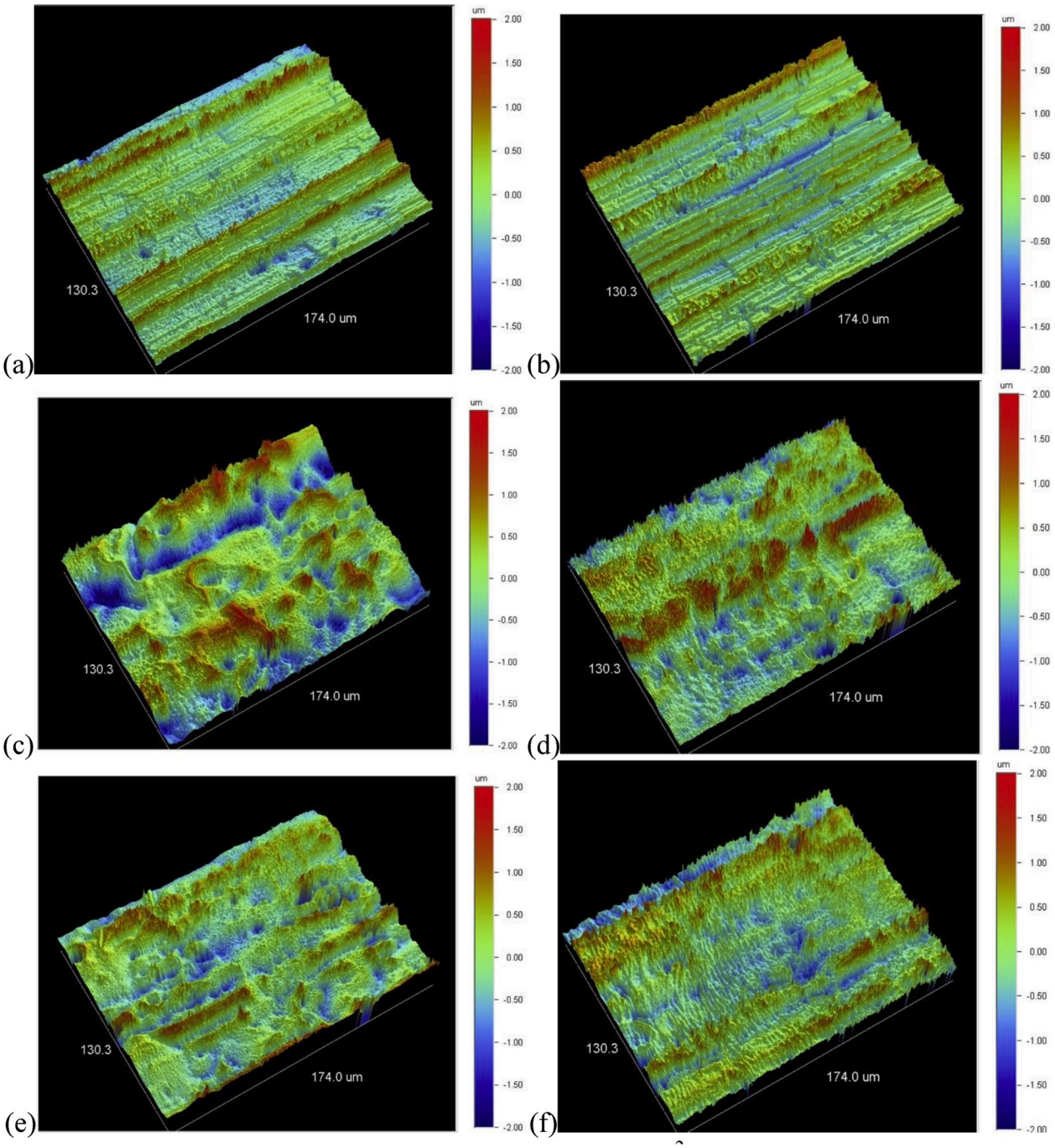

Fig. 1. Surface profiles at a laser fluence of $F_1 = 1.238$ J/cm^2 per pulse for (a, b) the as-received specimens and in typical centerlines of a laser scan for raster speeds of: (c) 2 mm/s, (d) 4 mm/s, (e) 6 mm/s, and (f) 8 mm/s.

images obtained with the profilometer are shown only for a quarter of the profiling surface, covering an area of 65 × 87 μm. The exact quarter where each optical micrograph was taken is indicated with two letters that indicate the position of the optically imaged area in the overall profiling area, namely LL, LR, TL, and TR for lower-left, lower-right, top-left, and top-right, respectively.

As evidenced by Figs. 1a, 2a and 1b, and 2b, the as-received and unprocessed aluminum surfaces are not smooth at all, exhibiting grooves in the horizontal direction from the rolling operation, quite a few microcracks, and pin-holes. The grooves are evidenced by horizontal dark stripes while the pinholes by round, dark-like features. The microcracks are evidenced by the jagged like dark-lines between the rolling grooves and are more visible in the optical micrographs (Fig. 2a and b) than in the profilometry images.

The structuring induced by the laser-interference is evidenced by the very fine striations in the vertical direction, i.e., normal to the rolling direction (Fig. 1c and e for the 3D profilometry; and Fig. 2d and f in the optical micrographs). In spite of the relatively rough original surface, the structuring by the laser-interference is thus shown to be pretty robust. This observation is consistent with that reported by Sabau et al. [11] for the interference-induced structuring of Al5182 aluminum alloy, where the variation in the structuring quality was explained by the considerations related to the energy absorption and evaporation of surface contaminants, such as lubrication oils, in addition to the optical phenomena related to the non-smooth original surfaces.

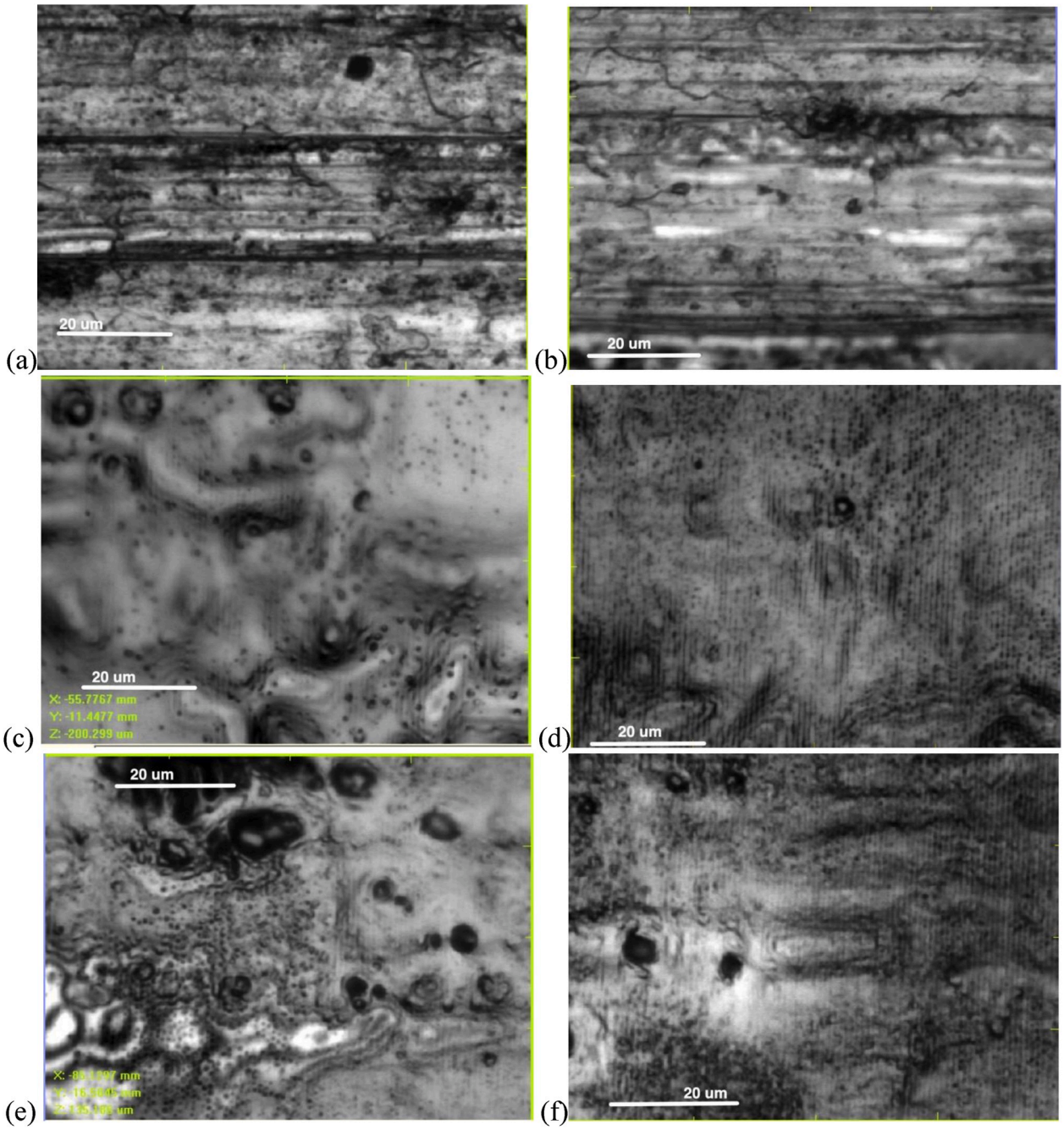

Fig. 2. Optical micrographs acquired by the profilometer. The corresponding location of the quarter area to the profilometry images shown in Fig. 1 is indicated in parenthesis: (a, b) the as-received specimens (TL, BL) and in the typical centerline of a laser scan for raster speeds of: (c) 2 mm/s (BL), (d) 4 mm/s (TR), (e) 6 mm/s (BL), and (f) 8 mm/s (TL). Laser fluence was $F_1 = 1.238$ J/cm^2 per pulse.

3.1. Results for roughness parameters

The average roughness, or arithmetical mean deviation of the roughness profile, R_a, root-mean-square deviation of the roughness profile, R_q, maximum roughness, R_z, and maximum height of the roughness profile, R_t, are shown in Table 3. As the height of the laser-interference structuring is expected to be less than 1.5 μm as shown by Lasagni et al. [10] while the R_z and R_t are on the order of 4–5 μm, the R_z and R_t are expected to be the least affected by the laser structuring. An increase in all surface roughness metrics can be observed between the indicators measured for the laser structured specimens with respect to the indicators measured for the as-received specimens, i.e., without any laser structuring. The increase in the surface roughness indicators with

Table 3
The surface roughness at a fluence of $F_1 = 1.238$ J/cm^2 per pulse.

Raster speed [mm/s]	R_a [nm]	R_q [nm]	R_z [μm]	R_t [μm]
[a]0	311.9	394	4.3	4.98
2	483.5	611.1	4.61	5.12
4	382.3	511.6	5.29	5.81
[a]0	282.5	358.9	4	4.87
6	334.6	439.9	5.79	7.45
8	359.4	442	5.26	6.15

[a] As-received, without any laser processing.

respect to that of the unprocessed condition, i.e., $dR[\%] = 100\left(R/R_O - 1\right)$, is shown in Table 4. The mean deviations of the roughness profile (R_a and R_q) were found to increase for all of the laser structured conditions by approximately 20–50%.

3.2. Results for LIS surface area

As evidenced by the profilometry data, LIS increases the surface area for adhesion. An attempt is made here to quantify the "roughness factor," r_{LIS}, to use same the terminology introduced by Wenzel [20] for coating adhesion. r_{LIS} is thus defined as the ratio of the LIS solid surface area to the original and unprocessed surface area. For one laser pulse, the expected surface morphology is shown in Fig. 3 and would consist in alternating depressions unto the as-received surface (in regions of maxima interference laser power) and mounds over the as-received surface due to the solidification of the migrated liquid metal (from maxima power regions). These alternating depression-and-mound structures are generated by the freezing of the nanosecond Marangoni-induced metal flow as indicated by Lasagni et al. [10] and Sabau et al. [11]. For the raster mode, the surface is exposed to multiple laser pulses, as indicated by the number of equivalent pulses, N_P, in Section 2.2. As the regions of maxima power created by the interference may not be superimposed for successive laser pulses, and some of the mounds formed at previous pulses maybe partially remelted and liquid metal would be moved partially to the depressions and partially to the mounds. Thus, the resulting surface morphology may be more complex than that illustrated in Fig. 3. In order to estimate the surface area after LIS, the wetted perimeter of the depression-and-mound LIS in the direction normal to the structuring direction has to be evaluated. The following considerations and assumptions can be made based on experimental evidence of the LIS geometry from Lasagni et al. [10] and Fig. 2, as illustrated in Fig. 3: (a) per each periodicity interval, d, the LIS profile can be approximated by a trapezoid with a lower base, b, and top base, a, and height, h; for low fluences, there would be two mounds per periodicity as the mounds, which grow from each of the neighboring depressions, do not merge; (b) the trapezoid shape is considered to be weakly dependent on the fluence, as the LIS induced depressions and mounds are based on migrating/spreading of the Marangoni-induced liquid metal and freezing it in place after the 2–3 ns pulse, hence the ratio a/b is considered to be fixed at 0.5; (c) $h(F,U)$ varies with fluence and raster speed U (through N_P); (d) the base size, b, was considered to be fixed at ~0.5d (as it can be inferred from Fig. 2). To summarize, the roughness factor can be calculated, as:

$$r_{LIS}(F,U) = 1 + \frac{b}{d}\left[2\sqrt{\frac{1}{4}\left(\frac{a}{b}-1\right)^2 + \left(\frac{h(F,U)}{b}\right)^2} + \frac{a}{b} - 1\right], \quad (4)$$

with a/b=0.5and b/d=0.5.

The height of the first "interference" mound, i.e., after one laser pulse, h_1, depends on the fluence. For one laser pulse, the h_1 was considered to be 0.05 and 1.2 μm for fluences of 1.24 and 1.78 J/cm^2, respectively, as indicated by Lasagni et al. [10] for pure Al. Several observations can be made to offer a glimpse in the variation of h with respect N_P (and consequently with U). For subsequent laser pulses, the same Marangoni forces as those at previous pulses would move less and less molten metal over the uphill slope of the mound; hence the incremental increase in the mound height, Δh_i, for each pulse, i, would decrease with each subsequent pulse (i.e., $\Delta h_{i+1} < \Delta h_i$). Also, the larger h_1, the smaller Δh_i is expected to be, as it more kinetic energy would be required to push the liquid metal uphill for larger mounds. To qualitatively estimate $h(F,U)$, it is assumed that $\Delta h_{i+1} = \beta(F)\,\Delta h_i$ and that β is 0.5 and 0.8 for fluences of 1.78 J/cm^2 ($h_1 = 1.2$ μm) and 1.24 J/cm^2 ($h_1 = 0.05$ μm), respectively. With these assumptions, $h(F,U)$, can be calculated, as:

$$h(F,U) = h_1(F)\frac{1-\beta(F)^{N_P(U)}}{1-\beta(F)} \quad (5)$$

The calculated values for $h(F,U)$ and r_{LIS} are shown in Table 5. For comparison, r_{LIS} for the first pulse was estimated to be 1.014 and 2.18 for fluences 1.24 and 1.78 J/cm^2, respectively. As expected, h and r_{LIS} exhibited weaker variation with N_P (and U) especially at medium/high fluences (e.g., 1.78 J/cm^2 with $h_1 = 1.2$ μm) than those at low fluences (e.g., 1.24 J/cm^2 with $h_1 = 0.05$ μm). The U-dependence of r_{LIS} is weaker at lower U values (4–6 mm/s) and weaker at the larger fluence of 1.78 J/cm^2 r_{LIS} is smallest at highest speed (10 mm/s). This qualitative data will be used further on to understand the effect of raster speed on the coating adhesion.

Table 4
The percentage increase in surface roughness metrics with respect to those for the as-received condition at a fluence of $F_1 = 1.238$ J/cm^2 per pulse.

Raster speed [mm/s]	dR_a [%]	dR_q [%]	dR_z [%]	dR_t [%]
2	55	55	7	2
4	22	29	23	16
6	18	22	44	52
8	27	23	31	26

*as-received, without any laser processing.

4. Results for coating adhesion testing

Before proceeding to the presentation of the coating adhesion results, the process variables related to the laser processing and coating application are presented. The coating Adhesion Rating (AR) depends on the laser fluence, F_1, laser raster speed, U, coating thickness, CT, and storage open-time, t_o. In short notation, AR is a function of four variables (F_1, U, CT, t_o). As a proof-of-principle investigation, this study was limited to few combinations of process parameters. In this study, the number of conditions and ranges for the process parameters, which were investigated, include: (a) two values for F_1 of 1.24 and 1.78 J/cm^2, (b) four raster speeds U of 4, 6, 8, and 10 mm/s; and (c) three open times of 20, 70, and 228 days at which the number of data was larger than five. The values selected for the fluence and raster speeds were based on the study by Sabau et al. [11] on another Al alloy.

For these conditions, most of the data was available for a coating thickness range of 15–23 μm (the nominal recommended coating thickness by the primer supplier is 15–30 μm with a mean of approximately 23 μm). Moreover, the adhesion results from the panels with the average coating thickness larger than the mean value of 23 μm that is specified by the manufacturer are briefly presented in the appendix. The number of conditions were identified in Table 6, where the selection of process parameters for the three analyses conducted in this study are shown.

4.1. Results for coating adhesion testing

All primer adhesion results discussed in this section were obtained from the panels with the average thickness of the coating of 15–23 μm; investigating the coating adhesion rating dependence on the other three variables (F_1, U, t_o). For most conditions investigated, the Adhesion Rating (AR) was measured for at least five specimens per each condition. The AR results can be presented either in a raw format, such as histogram, which counts the number of measurements that have a certain rating, or as an average. The average was applied to the measurement set using several filters. For example, the average adhesion rating over a given coating thickness range can be defined for each laser fluence, F_1, raster speed, U, and open time, t_o, as:

$$\overline{AR}1(F_1, U, t_o) = AVE[AR(F_1, U, CT, t_o)] \ for \ 15\mu m < CT < 23\mu m \quad (6)$$

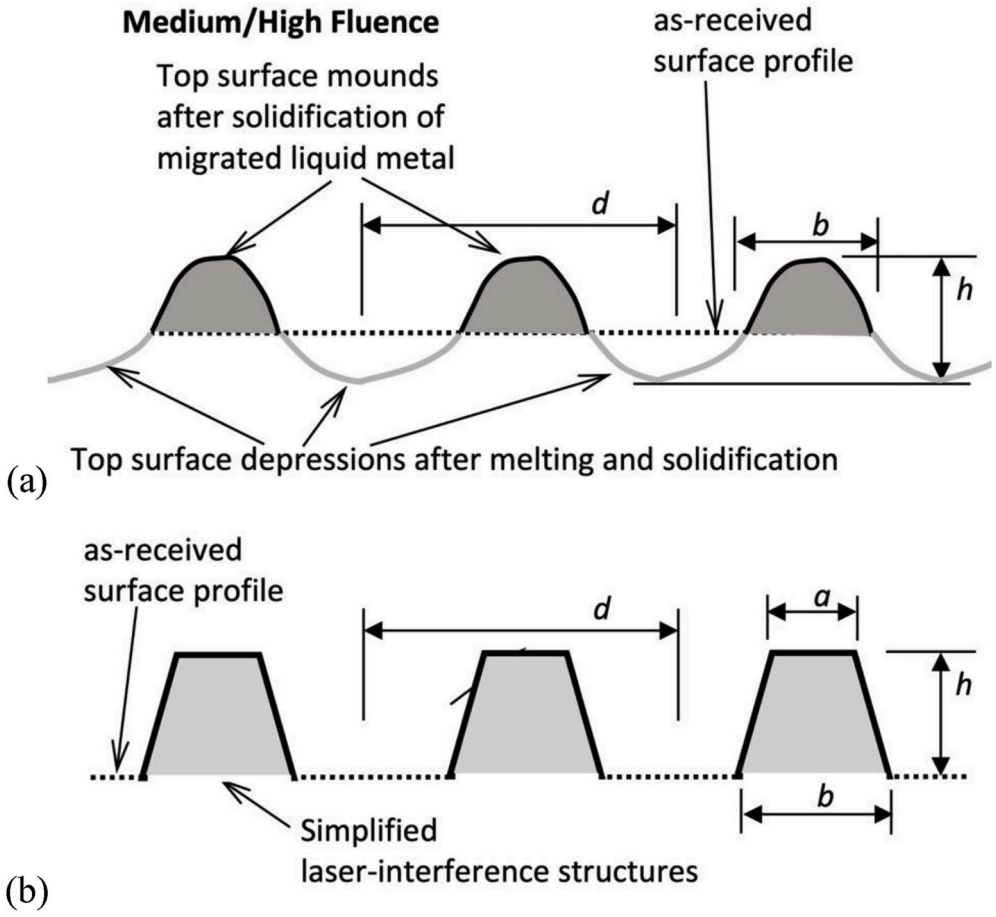

Fig. 3. Schematic of: (a) LIS surface topology and (b) simplified surface profile.

Table 5
Estimated LIS height, h, and roughness factor, r_{LIS}, for several raster speeds.

F_1 [J/cm^2]	1.238			1.782		
U [mm/s]	N_P	h [um]	r_{LIS}	N_P	h [um]	r_{LIS}
4	15	0.24	1.26	13	2.40	3.58
6	10	0.22	1.23	8	2.39	3.57
8	7	0.20	1.18	6	2.36	3.54
10	6	0.18	1.16	5	2.33	3.50

Table 6
Selection of process parameters for three analyses conducted.

Parameters Investigated	F_1 [J/cm^2]	U [mm/s]	CT [μm]	t_o [days]	No. data sets
Fluence and speed	1.24 and 1.78	4, 6, 8, and 10	15 to 23	All data	2x4
Open time	1.24 and 1.78	4 and 6 combined	15 to 23	Six values	6
Coating thickness	1.24	4, 6, 8, and 10	15 to 23, 23 to 30, and 30 to 44	All data	3

First, the results for the X-cut adhesion test are presented. Pictures of selected LIS panels after X-cut adhesion tests are shown in Fig. 4. The average primer thickness and the adhesion rating, from 0A, 1A, 2A, 3A, 4A, or 5A, are indicated at the bottom of each picture. It would have been more appropriate to assign fractional ratings of 4.5A and 3.5A for the panel shown in Fig. 4(b) and (c), respectively, based on the fact that its rating was considered to be below the 5A but definitely above the 4A.

Pictures of selected Al control panels after X-cut adhesion test are shown in Fig. 5. For the CCC control specimens, the X-cut rating was found to exhibit a large variation, from 5A for the specimen shown in Figs. 5a–1A for the specimen shown in Fig. 5c.

Second, the results for the cross-hatch adhesion tests according to ASTM D3359, Section 12, are presented. Pictures of selected cross-hatch adhesion test are shown in Figs. 6 and 7 for six laser-structured specimens and four control specimens, respectively. It would have been more appropriate to assign a fractional rating of 4.5B for the LIS panel shown in Fig. 6d, based on the fact that its rating seemed to be below the 5B but definitely above the 4B. Pictures of selected cross-hatch adhesion test for five control specimens, three specimens prepared with CCC and two specimens prepared by SAA are shown in Fig. 7. The coating adhesion of LIS specimens is very good, with some specimens exhibiting the highest coating adhesion rating. Moreover, the cross-hatch test rating of coated LIS specimens outperforms that of the control specimens, which were prepared with CCC.

The results for all of the X-cut and cross-hatch coating adhesion tests, which were conducted on coupons for which the coating thickness was between 15 and 23 μm, are summarized in Fig. 8a and b, respectively, for LIS, CCC, and SAA coated panels. In this histogram data, the ratings were combined for all coating sessions, i.e., irrespective of the open-time. The histograms shown in Fig. 8 indicate the number of data per each coating adhesion rating, AR, for each laser fluence, F_1, and each raster speed, U. The data shown with empty symbols and solid symbols are for LIS panels with a the laser fluence of 1.78 and 1.24 J/cm^2, respectively. As the X-cut test is considered in industry as a less severe test than the cross-hatch test, more specimens were tested for the cross-

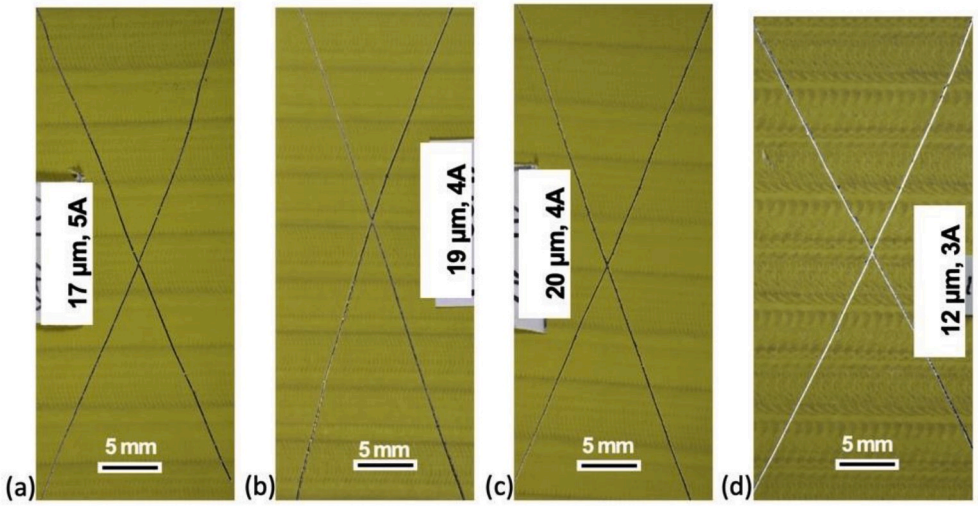

Fig. 4. Pictures of X-cut tested laser-structured Al panels at rastering speeds of (a–c) 4 mm/s and (d) 10 mm/s at a laser fluence of $F_1 = 1.238$ J/cm^2 per pulse. Coating thickness and X-cut test score according to ASTM D3359, section 7, are indicated for each figure.

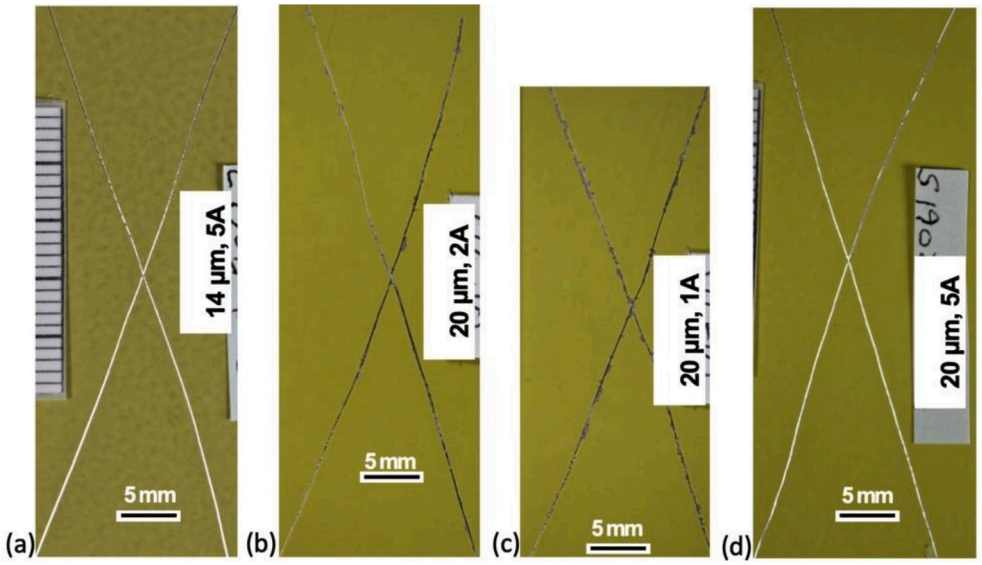

Fig. 5. Pictures of X-cut tested Al panels prepared with (a–c) CCC and (d) SAA treatments. Coating thickness and X-cut test score according to ASTM D3359, section 7, are indicated for each figure.

hatch test than for the X-cut test, once the laser structured specimens would pass this test.

For the data shown in Fig. 8a, the total number of X-cut tests was 4 and 16 for specimens prepared with laser fluences of 1.78 J/cm^2 and 1.24 J/cm^2, respectively. The calculated average X-cut ratings were 3.3A and 5A for the CCC and SAA controls, respectively. For the laser structured panels with laser fluence of 1.24 J/cm^2, the calculated average X-cut ratings were 4.6A, 4.5A, 5A, and 3.7A for 4, 6, 8, and 10 mm/s raster speeds, respectively. For the X-cut test, the SAA panels exhibited the highest adhesion rating while CCC panels showed a spread in the rating indicating quite a variation in the adhesion. Among all of the laser-structured conditions, the LIS panels with 10 mm/s raster speed exhibited the lowest rating; however, the average rating for this condition was still above that of the CCC panels. The average X-cut adhesion rating for the LIS surface treatment with 4, 6, and 8 mm/s was comparable to that for SAA surface treatment panels and higher than that for the CCC panels.

The results of cross-hatch coating tests of primer-coated Al panels are summarized in Fig. 8b. For the data shown in Fig. 8b, the total number of cross-hatch tests was forty-one and thirty-six for laser fluences of 1.78 and 1.24 J/cm^2, respectively. The statistical analysis of the cross-hatch test data shown in Fig. 8b is now presented. Several statistical Student t-Tests were conducted for the cross-hatch AR. The statistical analysis was performed using the Kaleidagraph software [21] by calculating Satterthwaite's approximate *t*-Test; a method in the Behrens-Welch family for unpaired data with unequal variance as indicated by Armitage and Berry [22]. The following variables were computed for each test of unpaired data (xi; i = 1, N and yj; j = 1, M) with unequal variance student *t*-Test, as given by Armitage and Berry [22]: mean values ($\overline{X}$ and $\overline{Y}$), mean difference ($\overline{X} - \overline{Y}$), standard deviations ($\sigma_x$ and σ_y), t-Value $t = (\overline{X} - \overline{Y})/s_{\overline{\Delta}}$ with $s_{\overline{\Delta}} = \sqrt{\sigma_x^2/N + \sigma_y^2/M}$, degree of freedom (DOF) as given by the Welch-Satterthwaite equation, and the two-tail (or two-sided) P-value. This P-value, or calculated probability, is the probability of finding the observed value "equal to or more extreme than what was actually observed." In our case, we used the Student t-Tests to determine if there is a statistically significant difference between the two means compared. If this P-value would be below a certain level (e.g.,

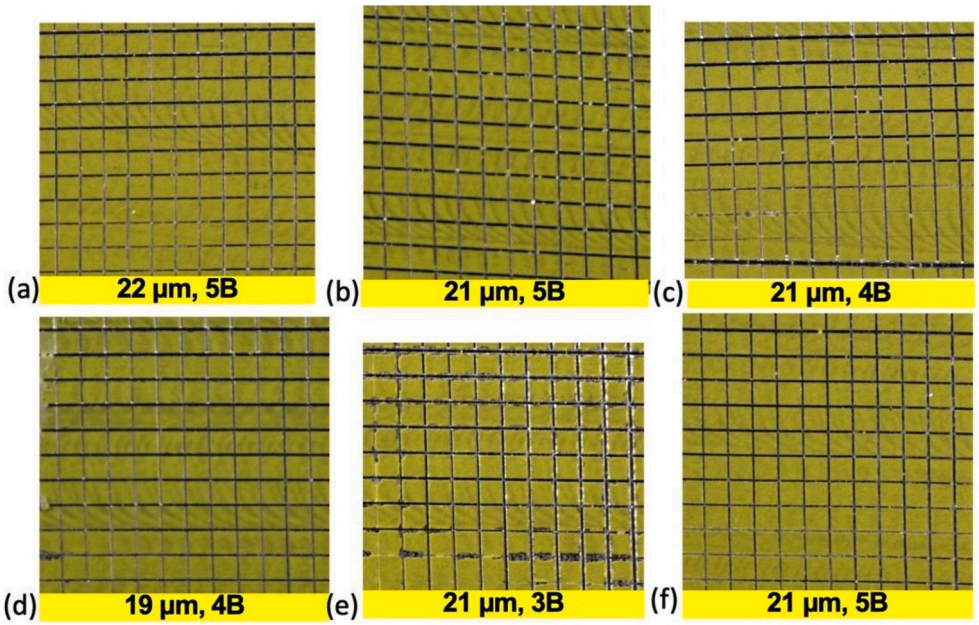

Fig. 6. Pictures of cross-hatch tested laser-structured Al panels, test scores (ASTM D3359, section 12), and coating thickness at rastering speed of (a–c) 6 mm s^{-1} and (d–f) 8 mm s^{-1} at a laser fluence of $F_1 = 1.782$ J/cm^2 per pulse. Grid size is 1 mm × 1 mm.

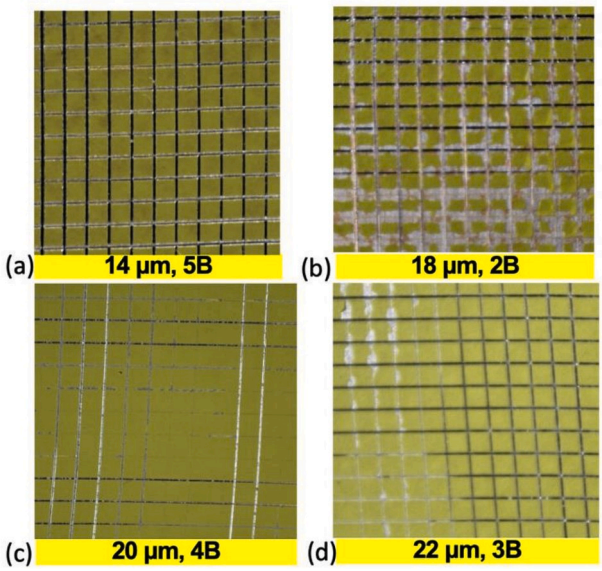

Fig. 7. Pictures of cross-hatch tested Al panels test scores (ASTM D3359, section 12), and coating thickness for (a, b) CCC and (c, e) SAA treatments. Grid size is 1 mm × 1 mm.

0.05 or 0.01), the conclusion would be that there would be a difference between the two group means, difference which would be statistically significant at the 95% or 99% confidence level, respectively.

The first Student *t*-Test was used to statistically compare the differences in AR between LIS(1.24 J/cm^2) and LIS(1.78 J/cm^2) at each laser speeds. As shown in Table 7, the t-Tests results indicate with 99% confidence level that each of the following datasets means are statistically different: (a) AR (1.24 J/cm^2, 6 mm/s) and AR (1.78 J/cm^2, 6 mm/s), (b) AR (1.24 J/cm^2, 10 mm/s) and AR (1.78 J/cm^2, 10 mm/s), and (c) AR (1.24 J/cm^2, all speeds) and AR (1.78 J/cm^2, all speeds). Here the "all speeds" was used to indicate lumped data for all the speeds. The means for data sets with LIS with 6 and 10 mm/s are not statistically different. The second Student *t*-Test was used to statistically compare the differences in AR data between SAA and LIS(1.78 J/cm^2). As shown in Table 8, the t-Tests results indicate that for all of the individual laser speeds (except 6 mm/s) the AR means for LIS 1.78 J/cm^2 are not statistically different than those for the AR with SAA. The mean values for 6 mm/s LIS at 1.78 J/cm^2 are statistically different than the mean for SAA as the mean for this LIS conditions is significantly higher than that for the SAA.

5. Discussion

Having established based on the mean values that LIS(1.24 J/cm^2) and LIS(1.78 J/cm^2) are mainly statistically different and that LIS(1.78 J/cm^2) and SAA (the highest AR for the control specimens) are statistically identical, an analysis of the AR data is made in order to study possible correlations for the coating adhesion performance to the laser processing space. Coating adhesion rating data can be also analyzed by averaging the data for each of the variables considered. The adhesion results from both X-cut and cross-hatch tests are summarized for the average and minimum adhesion ratings, AR, in Table 9. Due to the limited number of data for the X-cut test, the average shown was the proper average for the two laser fluences used instead of showing the averages per each fluence. For the cross-hatch test, both averages at the two laser fluences are shown in Table 9. The standard deviation is also shown for the cross-hatch ratings for the specimens prepared with the two laser fluences of 1.24 and 1.78 J/cm^2. Using the 2 σ as a 95% confidence level interval, for an assumed student t-distribution of the ratings, the Lower Confidence Limit (LCL) of the mean was calculated and it is shown in Table 9. The LCL can be used as a design basis value for the coating adhesion which represents the minimum value above which 95% of the coating adhesion ratings would be expected, i.e., minimum property values that would be reached with 95% confidence. For all the speeds, but the 8 mm/s, the LCL is higher for LIS at 1.78 J/cm^2 fluence than those at 1.24 J/cm^2 fluence. At 1.78 J/cm^2 fluence, for all of the speeds, but the 8 mm/s, the LCL is larger than 3, value which is close to that for the LCL of 2.8 for SAA. At 1.24 J/cm^2 fluence, the LCL is higher than 3 only for the 8 mm/s. Thus, more laser speeds were found to yield a higher LCL than the SAA at the 1.78 J/cm^2 fluence than at the 1.24 J/cm^2 fluence. A wider laser processing space was found at the 1.78 J/cm^2 fluence than at the 1.24 J/cm^2 fluence.

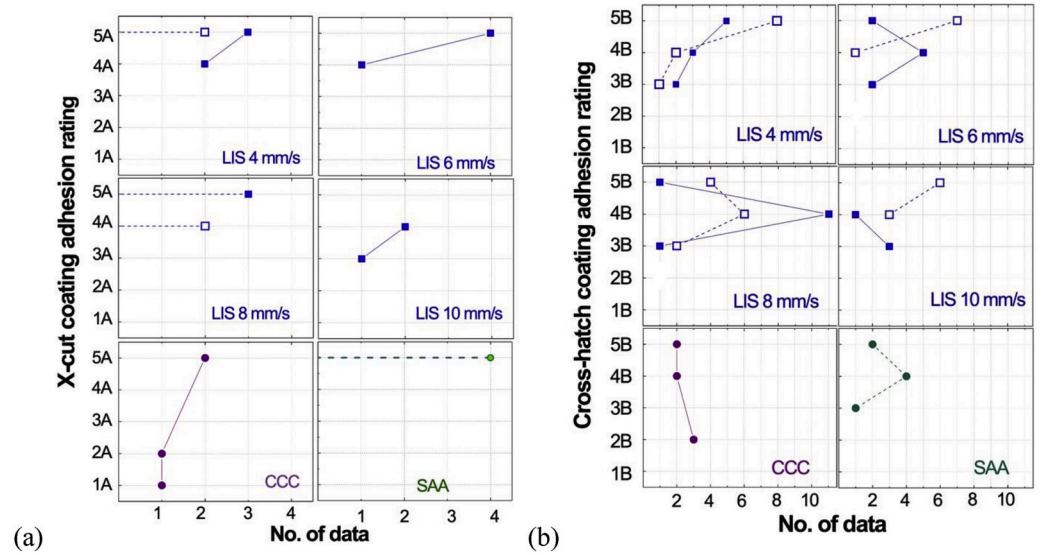

Fig. 8. Histograms for coating adhesion rating for LIS, CCC, and SAA coated panels for the: (a) X-cut and (b) cross-hatch tests. The solid symbols and empty symbols indicate data obtained at fluences F_1 of 1.238 and 1.782 J/cm^2 per pulse, respectively.

Table 7
Statistical results from Student t-Tests for individual pairs (LIS-LIS) of cross-hatch ratings at fluences of 1.78 J/cm^2 and 1.24 J/cm^2 at each rastering speed.

Rastering Speed [mm/s]	Mean difference	DOF	t Value	P-value	[a]Statistically different
4	0.34	17	1.02	0.322	–
6	0.88	12	3.28	0.00655	Y
8	0.17	17	0.706	0.49	–
10	1.42	5	4.72	0.00354	Y
All	0.49	74	3.01	0.00356	Y

[a] Statistically significant at the 99% confidence level, i.e., with P-value < 0.01.

Table 8
Statistical results from Student t-Tests for individual pairs (SAA-LIS) of cross-hatch ratings. LIS data was at fluences of 1.78 J/cm^2.

Rastering Speed [mm/s]	Mean difference	DOF	t Value	P-value	Statistically different
4	0.42	12	1.27	0.2283	N
6	0.66	8	2.26	0.0513	[a]Y
8	−0.048	12	−0.142	0.8894	N
10	0.45	10	1.45	0.1767	N
All	0.27	8	0.948	0.3694	N

[a] Close to be statistically different at the 95% confidence level, i.e., with P-value < 0.05.

Based on the X-cut and cross-hatch ratings, surfaces prepared with LIS, at rastering speeds of 4, 6, and 8 mm/s, and anodizing treatment provided similar adhesion performance, which was higher than that of the CCC Al surfaces. Concerning the rastering speed effect on cross-hatch ratings, the following considerations can be made based on the data shown in Table 9:

- The average rating for a laser fluence of 1.24 J/cm^2 is highest at the lowest rastering speed (4 mm/s), however, the ratings at the 4 and 6 mm/s are very close to each other,
- The average rating for the laser fluence of 1.24 J/cm^2 does not vary significantly as the raster speed is increased to 6 and 8 mm/s,
- The average rating for the laser fluence of 1.24 J/cm^2 is lowest at the highest rastering speed (10 mm/s),
- The average rating for the laser fluence of 1.78 J/cm^2 is highest at the rastering speed of 6 mm/s; however, the ratings at the 4 and 6 mm/s are very close to each other,
- With the exception of the 8 mm/s series of specimens, the average rating for the laser fluence of 1.78 J/cm^2 does not vary significantly for the other rastering speeds, and it is higher than those for laser fluence of 1.24 J/cm^2,
- The average rating for the laser fluence of 1.78 J/cm^2 is the lowest at the rastering speed of 8 mm/s,
- Overall, the lower confidence limit for the ratings at a laser fluence of 1.78 J/cm^2 were higher than those ratings at laser fluence of 1.24 J/cm^2,
- The highest ratings, and with the smallest standard deviation, were found for the laser fluence of 1.78 J/cm^2 and lower rastering speeds (4 mm/s and 6 mm/s).

Thus, based on the above analysis, the rastering with either 4 mm/s or 6 mm/s with a laser beam setup at a laser fluence of 1.78 J/cm^2 is recommended to attain acceptable coating adhesion, even higher than that with the anodizing surface treatment.

For the sake of completion, the adhesion rating results for specimens with different open times and different coating thicknesses are shown in Appendix A. Although there was not a dedicated effort to systematically investigate the storage open time effect, the data shows that the adhesion of primer after 200 days was still high, above 3.8 rating, and not significantly decreased compared to that for the shortest open time (20–21 days) investigated, indicating that LIS would allow extended open time for the application of CA7233 primer. Next, the coating adhesion rating for panels with the average coating thickness larger than the mean value of 23 μm that is specified by the manufacturer are discussed in Appendix A. In general, the coating adhesion rating is expected to be lower with increased coating thickness. The data showed that the thick-coated specimens exhibited moderate coating adhesion. These coating adhesion test results for thickest coatings, which are approximately 40–44 μm thick, almost as twice as large from desired coating thickness, were reported in Appendix A only as further evidence of the excellent coating adhesion exhibited by the laser-structured specimens.

The coating adhesion would depend on the surface cleanliness, surface energy, and actual topology of the surface and a correlation of the coating adhesion performance to the laser processing space can be inferred by tracking these important factors. The cleaning of the Al 2024 alloy surface from the surface contaminants due to lubrication oils from

Table 9
Average, minimum, and lower confidence limit adhesion ratings from X-cut and cross-hatch tests for LIS, CCC, and SAA panels coated with CA7233 primer.

Al surface treatment	Rastering Speed [mm/s]	X-cut rating (both fluences)		Cross-hatch rating (F_1=1.24 J/cm^2)			Cross-hatch rating (F_1=1.78 J/cm^2)		
		Avg.	Min.	Avg.	LCL	Std-dev.	Avg.	LCL	Std-dev.
LIS	4	4.7	4	4.3	2.66	0.82	4.6	3.26	0.67
	6	4.8	4	4.0	2.58	0.71	4.9	4.2	0.35
	8	4.6	4	4.0	3.18	0.41	4.2	2.76	0.72
	10	3.7	3	3.25	2.25	0.5	4.67	3.67	0.5
LIS	All			4	2.64	0.68	4.55	3.07	0.74
CCC	N/A	3.3	1	3.6	0.64	1.48	3.6	0.64	1.48
SAA	N/A	5	5	4.2	2.8	0.7	4.2	2.8	0.7

prior rolling operations was observed by Meyer et al. [19] at a fluence of 1.24 J/cm^2. The XPS data shows that this laser technique is effective at removal of some surface contaminants, particularly for C which was modestly reduced for 2 laser pulses processing dramatically reduced for 8 laser pulses. It is expected that at the higher fluence of 1.78 J/cm^2 the cleaning would be even more efficient, i.e., requiring even fewer laser shots to clean the surface. Preliminary data on contact angle measurements for LIS surfaces at a fluence of 1.24 J/cm^2 were used to calculate the surface energies of ~30 mN/m for CCC and LIS surfaces with 2, 4, 6, and 8 pulses/spot and ~66 mN/m for SAA. This indicate that the wetting behavior indicate that LIS surfaces were compatible with CCC and that the wetting behavior exhibited a weak variation with respect to the number laser shots per spot (all smaller than 8). Concerning the topology variation with processing, the roughness factor for LIS surfaces, r_{LIS}, was qualitatively evaluated in Section 3.2. r_{LIS} was estimated to monotonically decrease with increasing U; being smallest at highest speed (10 mm/s). r_{LIS} is likely to exhibit a small variation with U, especially at lower U values (4–6 mm/s). Moreover, r_{LIS} is likely to exhibit a weak dependence on U at the higher fluence considered (1.78 J/cm^2). Finally, r_{LIS} is likely to be larger at the 1.78 J/cm^2 fluence than at the 1.24 J/cm^2 fluence. All of these findings enumerated in this paragraph indicate that CA would be likely to exhibit the following trends: (a) be higher at the lower end of the speed range considered (4–6 mm/s), (b) be lowest at the highest speed considered (10 mm/s), and (c) be higher at the 1.78 J/cm^2 fluence.

6. Conclusion

This work aimed to study a laser-based surface treatment as a non-chemical surface preparation for aerospace coating systems. Laser-interference structuring was conducted at several raster speeds and two laser fluences. The surface profile and ensuing roughness for unprocessed aluminum surfaces and the laser-interference structured panels was presented. The as-received and unprocessed aluminum surfaces are not smooth at all, exhibiting grooves in the horizontal direction from the rolling operation, quite few microcracks, and pin-holes. In spite of the relatively rough original surface, the structuring by the laser-interference is thus shown to be pretty robust. The mean deviations, with respect to the unprocessed aluminum surfaces, of the roughness profile R_a and R_q were found to increase for all of the laser structured conditions by approximately 20–50%.

The commercial CA7233 primer, which complied with MIL-PRF-23377 specification, was spray painted on the Al surface prepared with laser-interference structuring, conversion coating or sulfuric acid anodized. Chromated conversion coated (CCC) and sulfuric acid anodized (SAA) surface of Al 2024 were considered as baseline or control specimens to assess the coating adhesion performance. The adhesion of primer on Al surface with different treatments was assessed using the ASTM D3359 X-cut and cross-hatch tests. The total number of X-cut tests was four and sixteen for specimens prepared with laser fluences of 1.78 J/cm^2 and 1.24 J/cm^2, respectively. Based on the average X-cut adhesion rating, LIS treatment with 4, 6, and 8 mm/s on Al panels resulted in primer adhesion comparable to SAA and higher than CCC panels. Based on the X-cut and cross-hatch ratings, surfaces prepared with LIS, at rastering speeds of 4, 6, and 8 mm/s, and SAA treatment provided similar adhesion performance, which was higher than that of the CCC surfaces.

The total number of cross-hatch tests was forty-one and thirty-six for laser fluences of 1.78 and 1.24 J/cm^2, respectively. It was found that the average rating for laser fluences of 1.24 and 1.78 J/cm^2 were highest at 4 and 6 mm/s rastering speeds, respectively. Overall, the lower confidence limit for the ratings at a laser fluence of 1.78 J/cm^2 were higher than those ratings at laser fluence of 1.24 J/cm^2. It was found that the highest ratings, and with the smallest standard deviation, were found for the laser fluence of 1.78 J/cm^2 and lower rastering speeds (4 mm/s and 6 mm/s). Moreover, as the coating testing results indicate, the surface preparation by LIS was found to enable an extended storage of the specimens after the laser-structuring and before the spray coating operation.

In conclusion, the rastering with either 4 mm/s or 6 mm/s with a laser beam setup at a laser fluence of 1.78 J/cm^2 is recommended to attain acceptable coating adhesion, even higher than that with the anodizing surface treatment. Based on the data presented, laser-interference structuring was found to achieve the desired specification adhesion for the CA7233 primer.

Notice

This manuscript has been authored by UT-Battelle, LLC, under contract DE-AC05-00OR22725 with the US Department of Energy (DOE). The United States Government retains and the publisher, by accepting the article for publication, acknowledges that the United States Government retains a non-exclusive, paid-up, irrevocable, world-wide license to publish or reproduce the published form of this manuscript, or allow others to do so, for United States Government purposes. The Department of Energy will provide public access to these results of federally sponsored research in accordance with the DOE Public Access Plan (http://energy.gov/downloads/doe-public-access-plan).

Declaration of competing interest

None.

Acknowledgement

This research was sponsored by Strategic Environmental Research

and Development Program (SERDP), 4800 Mark Center Drive, Suite 17D03, Alexandria, VA 22350-3605, managed by U.S. Department of Defense, U.S. Department of Energy, and U.S. Environmental Protection Agency. This research was conducted at UT-Battelle, LLC, for the SERDP project WP-2743 "Laser-Interference Surface Preparation for Enhanced Coating Adhesion and Adhesive Joining of Multi-Materials." The authors acknowledge the technical support from Tom Naguy, Deputy Technical Director, Air Force Materiel Command, W–P AFB; Michael Casey Jones, Materials Engineer, W–P AFB; Rick Osterman and Stan Bean of M&P Solutions LLC, Pahrump, NV.

Appendix A. Effect of open-time and coating thickness effect on adhesion rating

First, the coating adhesion rating dependence of the storage open time is presented. For each laser fluence, the cross-hatch adhesion rating data for both the 4 mm/s and 6 mm/s were averaged together since their ratings were close and ordered according to the open time. The cross-hatch adhesion ratings at several open times are shown in Table A1 for the two laser fluences considered in this study. The number of ratings used to obtain each reported coating adhesion average is also indicated in Table A1. There were only few specimens at open times of 49 days and 235 days. Although there was not a dedicated effort to systematically investigate the storage open time effect, the data shows that the adhesion of primer after 200 days was still high, above 3.8 rating, and not significantly decreased compared to that for the shortest open time (20–21 days) investigated, indicating that LIS would allow extended open time for the application of CA7233 primer.

Table A1
The average cross-hatch rating for both 4 mm/s and 6 mm/s laser raster speeds at two fluences and several open times.

F_1 [J/cm^2]	1.238		1.782	
Open time [day]	Average Rating	No. of ratings	Average Rating	No. of ratings
20	–	–	4.9	16
49	4.5	2	–	–
70	3.8	11	–	–
228	4.8	5	–	–
235	–	–	3.7	3

The results of the average X-cut and cross-hatch tests were presented in Fig. A1 for all surface treatments considered and three coating thickness ranges, namely 15–23 μm, 23–30 μm, and 30–44 μm, at a laser fluence of 1.24 J/cm^2. For each coating thickness range, the datapoints were connected for all surface pretreatments in order better illustrate the coating thickness dependence. The data for the ratings were combined for all of the coating sessions, i.e., irrespective of the open-time. The average adhesion ratings were obtained from at least two specimens per each condition.

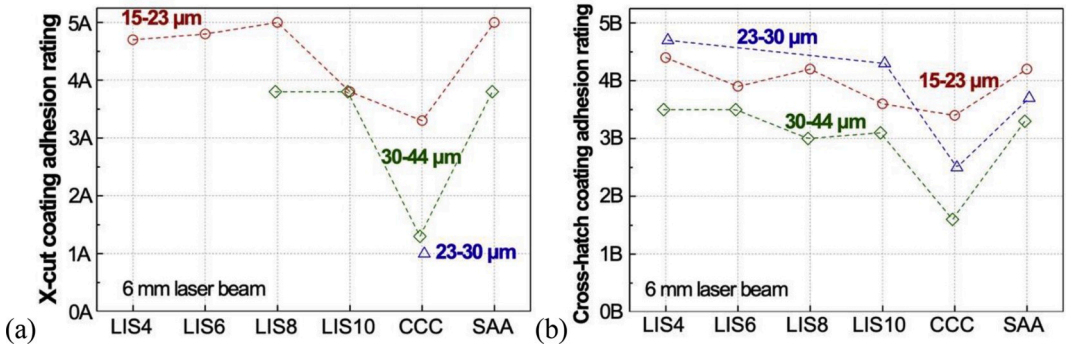

Fig. A1. Average adhesion ratings from (a) X-cut and (b) cross-hatch tests for different coating thickness for laser-structured at a laser fluence of $F_1 = 1.238$ J/cm^2 per pulse, CCC, and SAA panels. The digit in the LIS# indicate the rastering speed in mm/s.

Based on the X-cut test results, increased coating thickness resulted in lower adhesion on CCC, SAA, and some LIS panels. Similarly, cross-hatch test results also showed lowered adhesion in the primer coating thicker than 30 μm for all LIS surfaces as well as CCC and SAA surfaces. Moreover, the adhesion performance of the primer coating for the standard coated specimens (both 15–23 μm and 23–30 μm coating thickness) were not significantly different. These results are consistent with the vendor specifications that the thickness of primer coating should not exceed 30 μm in order to avoid reduction of adhesion performance.

References

[1] Brown GM, Kobayashi K. Nucleation and growth of a chromate conversion coating on aluminum alloy AA 2024-T3. J Electrochem Soc 2001;148:B457–66.
[2] Fukuda Y, Fukushima T. Anodic oxidation of aluminium in sulphuric acid containing aluminium sulphate or magnesium sulphate. Electrochim Acta 1983;28:47–56.
[3] González JA, López V, Otero E, Bautista A. Postsealing changes in porous aluminum oxide films obtained in sulfuric acid solutions. J Electrochem Soc 2000;147:984–90.
[4] Pearlstein F, Agarwala VS. Trivalent chromium solutions for applying chemical conversion coatings to aluminum alloys or for sealing anodized aluminum. Plat Surf Finish 1994;81:50–5.
[5] Campestrini P, Terryn H, Hovestad A, de Wit JHW. Formation of a cerium-based conversion coating on AA2024: relationship with the microstructure. Surf Coating Technol 2004;176:365–81.
[6] Critchlow GW, Brewis DM, Emmony DC, Cottam CA. Initial investigation into the effectiveness of CO2-laser treatment of aluminium for adhesive bonding. Int J Adhesion Adhes 1995;15:233–6.
[7] Langer M, Rechner R, Thieme M, Jansen I, Beyer E. Surface analytical characterisation of Nd:YAG-laser pre-treated Al Mg3 as a preparation for bonding. Solid State Sci 2012;14:926–35.
[8] Kai D, Parkhill RL, Wu J, Knoobe ET. Surface microstructuring of aluminum alloy 2024 using femtosecond excimer laser irradiation. IEEE J Sel Top Quant Electron 2001;7:567–78.
[9] Daniel C, Mücklich F, Liu Z. Periodical micro-nano-structuring of metallic surfaces by interfering laser beams. Appl Surf Sci 2003;208–209:317–21.
[10] Lasagni A, D'Alessandria M, Giovanelli R, Mücklich F. Advanced design of periodical architectures in bulk metals by means of Laser Interference Metallurgy. Appl Surf Sci 2007;254:930–6.

[11] Sabau S, Greer CM, Chen J, Warren CD, Daniel C. Surface characterization of carbon fiber polymer composites and aluminum alloys after laser interference structuring. J Occup Med 2016;68:1882–9.
[12] Meyer HM, Sabau AS, Daniel C. Surface chemistry and composition-induced variation of laser interference-based surface treatment of Al alloys. Appl Surf Sci 2019;489:893–904.
[13] Performance specification primer coatings: epoxy, high solids, MILPRF-23377K, june, vol. 7; 2012.
[14] Troconis CR, Frankel GS. Effect of roughness and surface topography on adhesion of PVB to AA2024-T3 using the blister test. Surf Coating Technol 2013;236:531–9.
[15] ASTM D4541-17. Standard test method for pull-off strength of coatings using portable Adhesion testers. 2017. West Conshohocken, PA.
[16] ASTM D3359-17. Standard test methods for rating adhesion by tape test. 2017. West Conshohocken, PA.
[17] Subasri R, Soma Raju KRC, Reddy DS, Jyothirmayi A, Ijeri VS, Prakash Om, Gaydos Stephen P. J Coating Technol Res 2019;16:1447.
[18] Alrashed MM, Jana Sadhan, Soucek Mark D. Corrosion performance of polyurethane hybrid coatings with encapsulated inhibitor. Prog Org Coating 2019; 130:235–43.
[19] Meyer HM, Sabau AS, Leonard DN. Laser-interference purse number dependence of surface chemistry and sub-surface microstructure of AA2024-T3 alloy, optics and laser technology. Submitted for publication; October 2019.
[20] Wenzel RN. Resistance of solid surfaces to wetting by water. Ind Eng Chem 1936; 28:988–94.
[21] Tellinghuisen J. Nonlinear least-squares using microcomputer data analysis programs: KaleidaGraph™ in the physical chemistry teaching laboratory. J Chem Educ 2000;77:1233.
[22] Armitage P, Berry G. Statistical methods in medical research. third ed. Blackwell; 1994.